Computational Materials Science 112 (2016) 96–106

Contents lists available at ScienceDirect

Computational Materials Science

journal homepage: www.elsevier.com/locate/commatsci

Diffusion properties of Fe–C systems studied by using kinetic activation–relaxation technique

Oscar A. Restrepo [a,d,*], Normand Mousseau [a], Fedwa El-Mellouhi [c], Othmane Bouhali [d], Mickaël Trochet [a], Charlotte S. Becquart [b]

[a] Département de physique, Université de Montréal, Case postale 6128, succursale centre-ville, Montreal, QC H3C 3J7, Canada
[b] Unité Matériaux et Transformations (UMET), Ecole Nationale Supérieure de Chimie de Lille, UMR CNRS 8207, Bat. C6, F59655 Villeneuve déAscq Cedex, France
[c] Qatar Environment and Energy Research Institute (QEERI), Hamad Bin Khalifa University, PO Box 5825, Doha, Qatar
[d] Texas A&M University at Qatar, Doha, Qatar

ARTICLE INFO

Article history:
Received 10 August 2015
Received in revised form 13 October 2015
Accepted 14 October 2015
Available online 19 November 2015

Keywords:
Defects
Diffusion
Activated dynamics
Kinetic Monte Carlo
Fe–C
Corrosion
Steel

ABSTRACT

Diffusion of carbon in iron is associated with processes such as carburization and the production of steels. In this work, the kinetic activation–relaxation technique (k-ART) – an off-lattice self-learning kinetic Monte Carlo (KMC) algorithm – is used to study this phenomenon over long time scales. Coupling the open-ended ART nouveau technique to generate on-the-fly activated events and NAUTY, a topological classification for cataloging, k-ART reaches timescales that range from microseconds to seconds while fully taking into account long-range elastic effects and complex events, characterizing in details the energy landscape in a way that cannot be done with standard molecular dynamics (MD) or KMC. The diffusion mechanisms and pathways for one to four carbon interstitials, and a single vacancy coupled with one to several carbons are studied. In bulk Fe, k-ART predicts correctly the 0.815 eV barrier for a single C-interstitial as well as the stressed induced energy-barrier distribution around this value for 2 and 4 C interstitials. For vacancy–carbon complex, simulations recover the DFT-predicted ground state. K-ART also identifies a trapping mechanism for the vacancy through the formation of a dynamical complex, involving C and neighboring Fe atoms, characterized by hops over barriers ranging from ∼0.41 to ∼0.72 eV that correspond, at room temperature, to trapping time of hours. At high temperatures, this complex can be broken by crossing a 1.5 eV barrier, leading to a state ∼0.8 eV higher than the ground state, allowing diffusion of the vacancy. A less stable complex is formed when a second C is added, characterized by a large number of bound excited states that occupy two cells. It can be broken into a V–C complex and a single free C through a 1.11 eV barrier.

1. Introduction

Properties of iron–carbon alloys (Fe–C) have been investigated extensively over the years, as these are crucial in carburization, steels and processes such as metal dusting corrosion [1]. However, in spite of years of studies, the microscopic details of C diffusion are still not fully characterized in part because of the time limits of standard atomistic simulations. On the one hand, flexible approaches, such as molecular dynamics, are limited to the micro-second time scale. On the other, long-time methods such as standard lattice kinetic Monte Carlo simulations [2,3] are constrained to lattice-based displacements that fail to capture the full diversity of diffusion mechanisms as well as elastic deformations. The recent development of on-the-fly off-lattice kinetic Monte Carlo methods such as the kinetic activation–relaxation technique (k-ART) [4–6] lifts those limitations and allows us to map these processes in details.

K-ART is an off-lattice kinetic Monte Carlo method with on-the-fly catalog building capabilities which properly handles elastic deformations and complex local environments such as ion-bombarded Fe [5,7] and Si [8], and amorphous Si [9]. As shown in a recent k-ART study of vacancy aggregation in Fe [10,11], even relatively simple systems require extensive cataloging and the exact handling of elastic effects on both energy minima and barriers to properly describe diffusion and aggregation kinetics in bcc Fe over experimentally-relevant time scales.

Until now, most numerical studies of interstitial C atom diffusion in Fe have used empirical MD [12–14], object KMC [15,16] and static DFT [17–21] to complement experimental

* Corresponding author at: Département de physique, Université de Montréal, Case postale 6128, succursale centre-ville, Montreal, QC H3C 3J7, Canada.
E-mail addresses: oa.restrepo.gutierrez@umontreal.ca (O.A. Restrepo), normand.mousseau@umontreal.ca (N. Mousseau).

http://dx.doi.org/10.1016/j.commatsci.2015.10.017
0927-0256/

results [22–28]. For instance the behavior of carbon–carbon (C–C) and carbon–vacancy (V–C) systems in iron has been studied using DFT by Domain and Becquart [29] who showed that interactions between two or more C interstitials or between C and self-interstitials are mainly repulsive, contrary to previous predictions by Johnson et al. [30]. These interstitials are trapped by vacancies, however, forming stable vacancy–C complexes. Each vacancy can bind up two C atoms. The complex becomes energetically unstable when three or more C atoms are present, a result that was corroborated by other DFT work [17]. These simulations suggest that C interstitial diffusion takes place through jumps between octahedral sites, with the barrier located at the tetrahedral sites. This mechanism would remain valid for V–C complexes, as C atoms migrate from one octahedral site to the next in one or two steps. In spite of these studies, there remains a considerable uncertainty regarding the magnitude and form of the migration path over long time, especially when it comes to the unbinding of the V–C, for which the precise diffusion mechanism is still lacking [12].

Effects of stress on these barriers have also retained attention. Recently, Tchitchekova et al. introduced a method called Linear Combination of Stress States (LinCoSS) to capture the effects of simple-heterogeneous uniaxial and shear stresses on the diffusion barrier of one C in Fe [31]. Energy barriers as a function of either uniaxial traction/compression and shear stress are determined with the Climbing Image-Nudge Elastic Band method (CI-NEB) and the EAM potential [32,33], they range from 0.7 to 0.9 eV for uniaxial stresses and from 0.75 to 0.83 eV for shear stresses of up to 3 GPa. Beyond these quantitative effects, pure shear could also move the saddle point position away from the tetrahedral site. Effects of internal stresses induced by the presence of more than one C atom in the barrier energy are still open, however.

Using k-ART with the *ab initio*-derived Becquart Fe–C potential [32,33], this paper addresses these issues and clarify the long-time diffusion mechanisms for C in Fe and the effect of internal stress in the presence and absence of vacancies. The paper is organized as follows: The computational method and potential used are described in Section 2. Section 3 is dedicated to validating the use of k-ART through the characterization of the diffusion properties in simple Fe–C systems as a function of temperature: one Fe vacancy and one C interstitial. In Section 4, we turn to more complex systems with two and four C interstitial atoms. In Section 5, systems with vacancy–carbon interactions are analyzed. Finally the conclusions are given in the last Section 6.

2. Methodology

2.1. An overview of k-ART

The main tool used here is the kinetic activation–relaxation technique (k-ART), a generic kinetic Monte Carlo algorithm designed to explore the energy landscape of complex atomistic systems, through the use of an off-lattice on-the-fly approach [4–6]. This method makes it possible to study the Fe–C kinetics on long time scales without restriction on the atom positions, exactly taking into consideration the full elastic effects.

While details of k-ART implementation can be found elsewhere [5,6], we summarize here its basic elements. At the beginning of each KMC step, the local environment surrounding each atom is evaluated using a topological approach and analyzed using the NAUTY package [34,35]. If the topology has already been visited, events associated with it are recovered from the catalog and placed in a KMC tree, otherwise, the catalog is updated by launching a series of ART nouveau searches to identify the diffusion mechanisms associated with this topology. Once the catalog is fully up-dated and the tree is completed for the current atomistic configuration, events are ordered according to their rate, defined as

$$r_i = \nu e^{-E_{b,i}/k_B T} \tag{1}$$

where the attempt frequency is fixed at $\nu = 10^{13}$ s^{-1} and $E_{b,i}$ is the barrier energy (also known activation energy) for event i, defined as the energy difference between the saddle point (sad) and the initial local minimum (min), $E_{b,i} = E_{sad,i} - E_{min,i}$ (in what follows index i is suppressed for simplicity).

All events that have a probability of at least 0.01% of occurring are fully reconstructed and reconverged. In this manner, low barriers are fully relaxed according to actual geometry and, therefore, exactly include short and long-range elastic effects. When this is done, rates are recomputed according to the real environment-specific environment, an event is chosen and the clock is brought forward according to KMC rules.

Since KMC simulations treat each step in series, its dynamics is dominated by the lowest energy barriers. To gently handle the small barriers that are responsible for flickering states (or states separated by small barriers and that do not allow the system to evolve), we use the basin-autoconstructing mean rate method (bac-MRM) which computes an on-the-fly statistically correct analytic solution of the connected flickering states and their escape rate as the energy landscape is explored [36,5].

2.2. Potential

We use an embedded-atom method type potential for describing the Fe–C system. Fe–Fe interactions are handled by the interatomic potential developed by Ackland and Mendelev [37], a potential that provides high agreement with DFT calculations. Fe–C interactions, developed by Becquart and collaborators, are also adjusted on *ab initio* calculations [32] with a special focus on the correct description of the activation barriers in order to ensure the right kinetics for C diffusion [33]. This potential has been used with success to model the effect of the stress field of an edge dislocation on carbon diffusion [38], the formation of carbon Cottrell atmospheres in bcc iron [39] as well as the elastic constants of the martensite [40]. Becquart's potential describes C–C interactions only through the embedded function, leaving aside short-range covalent C–C interactions. This approximation is valid for diluted solutions such as the ones studied here where C are not in first-neighbor positions and interaction through common Fe atoms or long-range elastic effects [32].

The potential is linked to k-ART package through the LAMMPS library, which is used as the force-calculation engine [41,42].

2.3. Simulation details

Simulations are based on a $8a_0 \times 8a_0 \times 8a_0$ 1024 Fe cubic bulk crystal with a_0, the lattice constant for bcc Fe crystal, set to $a_0 = 2.8553$ Å. C atoms and Fe vacancies are added according to the details of each simulation. All systems are run at temperatures of 300, 600, 900, 1100, and 1200 K to assess thermal effects on kinetic trajectories. As is normally the case in KMC simulations, the temperature is only used to choose the transition states according with the transition state theory [43,44] and all simulations are performed in the canonical ensemble with the volume set to ensure $P = 0$ at $T = 0$ K. The relevance of this approximation is examined in Section 3.3, where we look at the effect of thermal expansion on minimum and migration barriers.

Because of the small number of defects, we use here the total square displacement, $\mathrm{SD}(t_n)$, at time step t_n defined as

$$\mathrm{SD}(t_n) = \sum_{i=1}^{N} (r_i(t_n) - r_i(0))^2, \tag{2}$$

where N is the number of particles and $r_i(0)$ is the initial position of atom i at KMC step zero. No normalization to N, which would

provide the mean square displacement, is performed, since diffusion is totally dominated by the motion of the defects or their neighboring atoms, with the majority of the atoms remaining at their initial position.

For each simulation, the ground state (GS) energy is defined as the lowest energy minimum identified during the run, E_{GS}. For clarity, all energies are given with respect to the GS, i.e., $E(t_n) = E\prime(t_n) - E_{GS}$. Given the simplicity of the systems studied, E_{GS} is reproduced for all simulations on the same system, irrespective of the temperature or the initial state, unless noted. Following references [29,32], the binding energy is computed as

$$E_{bind}^{(A_1,\ldots,A_n)} = \sum_{i=1}^{n} E^{(A_n)} - [E^{(A_1,\ldots,A_n)} + (n-1)E_{ref}], \tag{3}$$

where $E_{ref} = -4109.294$ eV is the energy of the perfect crystal. Thus for two C interstitials the binding energy is given by $E_{bind}^{2C} = 2E_{GS}^{(1C)} - [E_{min}^{(2C)} + E_{ref}]$, while for V–2C complex, it is given by, $E_{bind}^{V2C} = 2E_{GS}^{(1C)} + E_{GS}^{(V)} - [E_{min}^{(V2C)} + 2E_{ref}]$. A positive E_{bind} means attraction.

3. Characterization of the Fe–C potential and validation of k-ART application to this system

To assess the efficiency of k-ART with the Fe–C EAM potential and establish point a comparison, we first look at the diffusion properties of two well-studied simple systems: a single Fe vacancy and a single C interstitial.

3.1. One Fe vacancy

As a first validation test, we look at the diffusion of a single Fe vacancy (V) (see Fig. 1). We will understand here a V as the absence of an atom from the a lattice site when compared to a perfect crystal. With this definition we consider that a vacancy V is created when an atom moves by more than 0.5 Å far from its lattice point, this definition is possible since KMC simulations do not include thermal displacements and focus on local minima and transition states. The formation energy, defined as the vacancy produced when removing one atom from the system, is defined as $[E_{GS} - (1023/1024)E_{ref}] = 1.721$ eV, with the EAM potential. Vacancy self-diffusion takes place between the {1 1 0} lattice planes through first-neighbor jumps, crossing an energy barrier, E_b, of 0.640 eV. This barrier leads either directly to an equivalent or to an intermediate interstitial position at $E_{min} = -0.549$ eV above the GS (at $E_{GS} = -4103.560$ eV). From this state a second barrier with energy of $E_b = 0.091$ eV brings the system back into a new GS (see Fig. 2). The 0.640 eV barrier is in agreement with the previously identified value [11,45], and the 0.091 eV barrier connecting the metastable state to the GS is close to the 0.12 eV value reported for both this Fe potential (named aA04) and a variation labeled A07 in [45]. The differences can be attributed to the convergence methods and the criteria used to find the saddle points. This split mechanism is not observed in DFT calculations and is considered to be an artifact of the EAM potential [45].

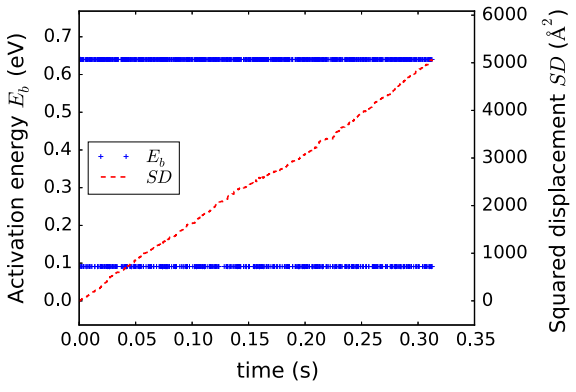

Fig. 1. Activation-energy (left, blue symbols) and squared displacement self-diffusion (right, red line) as a function of time for a single Fe vacancy in a bcc crystal at 300 K, over 1446 KMC steps. The self-diffusion is computed as a total square displacement of the Fe atoms (dashed red line). The blue dots indicate the selected activation barriers. Here, the vacancy diffuses in two steps: from a GS to metastable state at $E_{min} = 0.549$ eV by crossing a barrier energy of 0.640 eV (higher blue dots), from this state to a new GS site by crossing a barrier energy of 0.091 eV (lower blue dots). (For interpretation of the references to color in this figure legend, the reader is referred to the web version of this article.)

Note that while the 1.07 eV barrier corresponding to the third-neighbor split vacancy, already observed in Ref. [11], is present in the event catalog, it is never selected in our simulations due to its low probability.

We will return back to this system when we analyze one V–C interaction and diffusion properties in Section 5.1.

3.2. One C interstitial

We now turn to the characterization of the energy landscape for a single C interstitial.

In simulations running for up to 48 000 events, k-ART with the EAM potential is found to reproduce the relatively simple results of previous MD simulations. In particular, k-ART predicts correctly the dominant diffusion energy barrier, $E_{barr} = 0.815$ eV, in agreement with the value found by MD simulations [12,33]. The same mechanism is observed at all temperatures. In Fig. 3, we plot the C self-diffusion at 600 K and the activation energy E_b as a function of time, as well as the single-valued energy barrier. Results for higher temperature simulations show the same basic physics.

In the GS at $E_{GS} = -4119.352$ eV, the C atom occupies the octahedral interstitial position. The C diffusion pathway goes through the tetrahedral site, as the transition state, in agreement with *ab initio* calculations [29,46].

3.3. Effects of thermal expansion

As stated above, KMC simulations typically neglect the effect of thermal expansion on energy barriers. The impact of this approximation is considered here for the self-vacancy and one C interstitial.

We perform zero pressure MD calculations with the EAM potential to establish thermal expansion for this material. Between 0 and 1200 K, the zero pressure lattice parameter changes with temperature, as $a(T) - a_0 = 1.4914 \times 10^{-8} T(T + 792.008)$. According to this equation, the changes of the lattice parameter and volume with respect to their 0 K values are 0.436% and 1.314% at 600 K, and 1.249% and 3.793% at 1200 K respectively.

Using this formula, we relaunch a series of KMC simulations with temperature-corrected volumes with both the self-vacancy and one C interstitial. Effects on total minimum and migration energies are given in Fig. 4 as a function of T (bottom scale) and $a(T)$ (top scale). While, as expected, the effect of expansion on total energy for this 1024-atom system is on the eV scale, the important quantities are the migration barrier energies for both V and C, which change by less than 0.02 eV between 0 and 600 K, and 0.05 eV between 0 and 1200 K. This change is, as expected, in opposite directions as lattice expansion stabilizes free volumes such as vacancy while it does the opposition of interstitials, but remains small in both cases.

As we see, thermal expansion effects on energy barriers are small (~6% as maximum) and on the order of thermal energies in

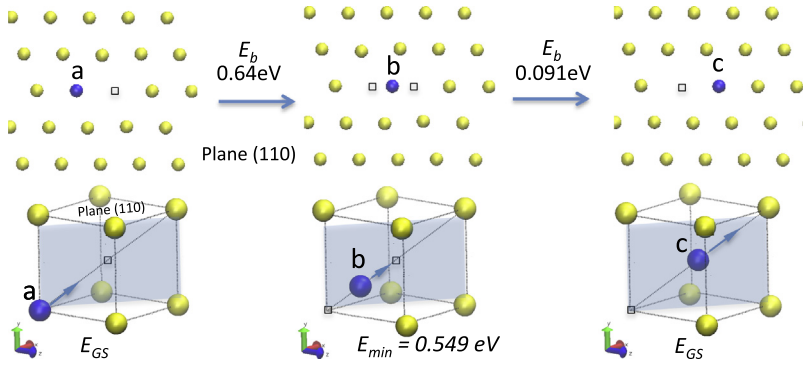

Fig. 2. Top: Schematic representation of the two possible transitions observed for a single Fe vacancy (square) into the planes {1 1 0}. Diffusion is done between nearest-neighbor atoms via $a \rightarrow c$, crossing a barrier of 0.640 eV (with no change in initial and final energies of the system), or via a split-step $a \rightarrow b \rightarrow c$, leading to a metastable state b with $E_{min} = 0.549$ eV. From $b \rightarrow c$ the system returns to a GS a site crossing a smaller barrier of 0.091 eV. Bottom: 3D view of the same configurations.

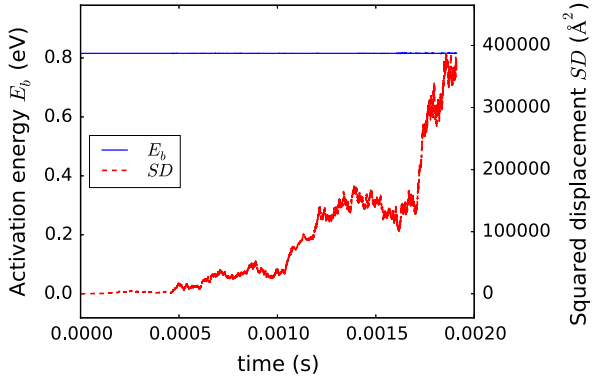

Fig. 3. Activation-energy (left, blue symbols) and squared displacement diffusion (right, red line) as a function of time for a 48909 KMC step single carbon interstitial run in a bulk system at 600 K. The migration energy of C is found to be 0.815 eV. (For interpretation of the references to color in this figure legend, the reader is referred to the web version of this article.)

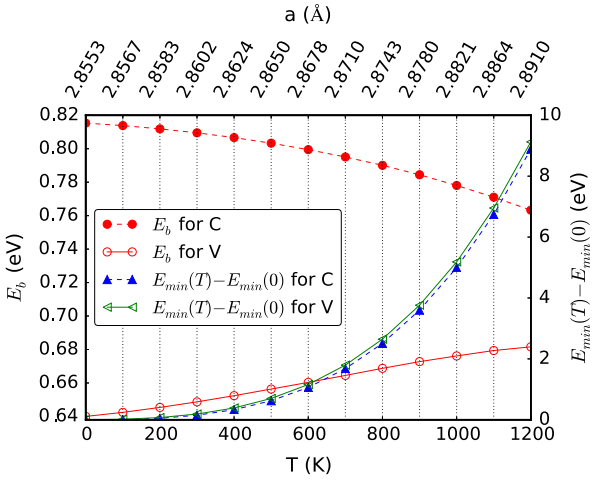

Fig. 4. Change of the $E_b(T)$ left, $(E_{min}(T) - E_{min}(0))$ right, and lattice parameter $a(T)$ top, with temperature T for systems: one vacancy V and one C atom. The variation of the lattice parameter follows a trend curve of quadratic form $a(T) - a_0 = 1.4914 \times 10^{-8} T(T + 792.008)$. For the V system the energy varies as $E_{min} - E_{GS} = K(a(T) - a_0)^2$ with $K = 7008.4$ eV/Å^2, and $E_b = -20.5652a(T)^2 + 119.3463a(T) - 172.4669$. For the C system E_{min} has the same form with $K = 7046.6$ eV/Å^2, and $E_b = -7.8536a^2(T) + 43.664a(T) - 59.8299$.

this system. They can therefore be neglected for the relatively simple configurations we are examining in this work.

4. Diffusion for systems with many interstitial C atoms

Having established that the single C-interstitial diffusion is well reproduced with k-ART/EAM, we consider in this section the effect of increasing the number of C impurities on the barrier energies. Here, we look, more specifically, at the diffusion mechanisms for dilute systems with two and four C interstitials, i.e. in the context where C-atoms are non in first-neighbor bonded-configurations. Results for higher temperatures are only discussed when they differ from those at 600 K.

4.1. Two C interstitials

We start by describing the GS configuration for the two C interstitial system. As shown in Fig. 5a, in the GS, the two C atoms are positioned in adjacent cells and separated by a distance of $\sqrt{3}a_0$ with an attractive binding energy of 0.045 eV with respect to two isolated C interstitials. This configuration has been previously observed in MD and DFT [29,32].

While the two carbon atoms are far apart, we recover the 0.815 eV characteristic of the single C diffusion, Figs. 6 and 7 show a rich behavior when the two C atoms come nearby each other, as they interact through elastic deformations of the Fe lattice (see, for example, at ~28 μs). In Fig. 6, we report the C-diffusion and the migration energy as a function of time for the full simulated time interval. While the 0.815 eV barrier, that characterizes the single C diffusion, dominates, fluctuations around this value demonstrate the effect of C–C interactions. A more detailed analysis is given in Fig. 7, which also shows the C–C distance evolution, d_{C-C}, as a function of KMC step, calculated for folded and unfolded trajectories, that is, using, or not, the nearest-image convention for computing the C–C distance. At each KMC step, the unfolded distance gives us the C–C separation of the same two C atoms as they move throughout any of the image boxes, while the folded distance provides the closest separation between two different C atoms (as we have two C atoms per volume box). These quantities are also compared to the square root of SD as well as to the migration energies and the energy at the local minima during the trajectory.

The complete distributions of activation energies and local minimum energies at the initial and the final states are plotted in the three histograms of Fig. 9. To follow the various events, each local energy state, binned with an energy resolution of 10 meV, is given a specific color in the top graph. This coloring makes it possible to identify the visited saddle (middle graph) and final configurations from each bin. For example, if the system is at state with initial energy ~0.09 eV above GS ($E_{GS} = -4129.455$ eV) (cyan), the system

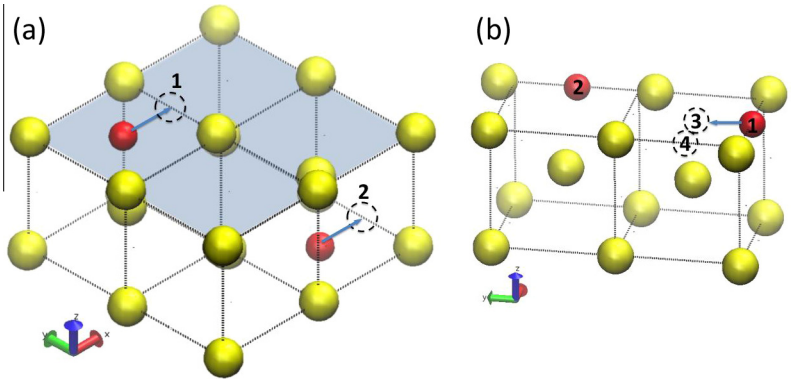

Fig. 5. Ground state configuration corresponding to the global minimum, E_{GS}, for 2C atoms. The two C atoms (red) are in the top (gray area) and bottom planes, separated by a distance of diagonal length of $\sqrt{3}a_0$. 1 and 2 represent another possible symmetric configuration of the GS. (b) Flickering states 3 and 4 for the C atom marked with 1 (see text for more details). (For interpretation of the references to color in this figure legend, the reader is referred to the web version of this article.)

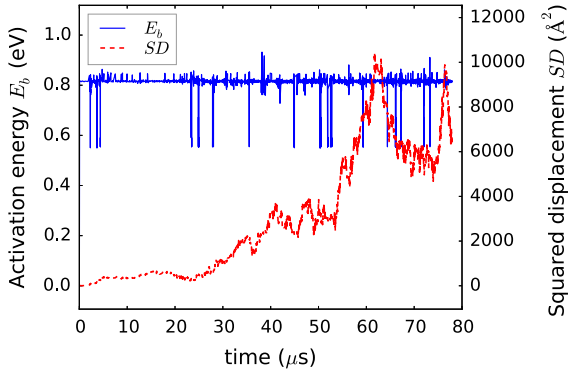

Fig. 6. Self-diffusion and migration energy for a Fe crystal with a two C interstitials at 600 K as a function of time for a 3814 KMC step run. The self-diffusion is computed as the total square displacement of the Fe atoms (dashed red line). The oscillations in the barrier energy (blue solid line) show the presence of different local minima. The lowest values of migration energy are metastable states in which the two C interact at short distance. (For interpretation of the references to color in this figure legend, the reader is referred to the web version of this article.)

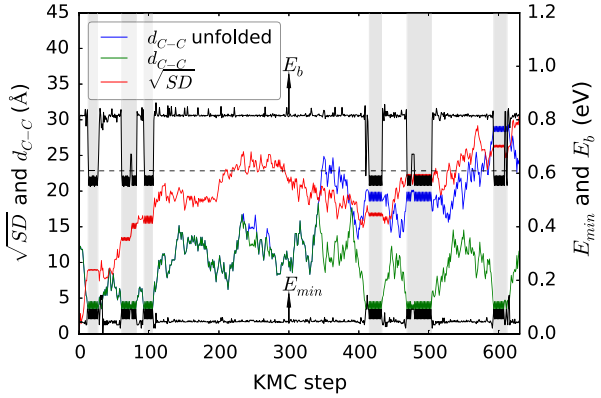

Fig. 7. Evolution of the C–C distance, d_{C-C}, (folded and unfolded, left axis), the square root of the squared displacement (SQ, left axis), the barrier energy E_{barr} and the energy at the local minima, E_{min} at 600 K as a function of KMC step (right axis). Grey strips represent the interval in which C–C are interacting and the dotted horizontal line is the box size: $8a_0$. This corresponds to time interval from 0 to 28.37 μs in Fig. 6.

can transit to a final state with energy ∼0.05 eV by crossing a barrier of 0.55 eV. Now if this state is taken as the initial one (pink), the system moves back by crossing a barrier of 0.59 eV.

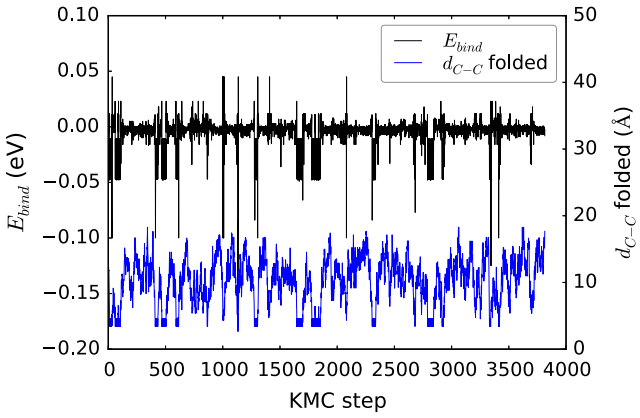

Fig. 8. Binding energy, E_{bind} (left axis), and distance for the two closest C atoms (d_{C-C} folded, right axis) as a function of KMC steps at 600 K.

Overall, we observe three diffusion regimes for the two C system. The dominant regime, associated to the state in green, at $E_{min} = 0.04$ eV above the GS, corresponds to the diffusion of isolated C atoms, crossing a 0.815 ± 0.05 eV barrier (with the error calculated as the half of the bin width of 10 meV).

The second regime, corresponding to the cyan and pink bins, corresponds to interacting trapped C atoms; these excited states are observed 215 times in the simulation, representing around 6% of the visited states. Trapping occurs when the two carbons are between 3.40 and 4.54 Å of each other (corresponding to roughly second and third neighbor position with respect to the bcc lattice in Fig. 5b), with repulsive C–C binding energies of −0.045 eV and −0.011 eV respectively. In that range, the carbon atoms can occupy a number of similar metastable positions, 0.055 eV and 0.092 eV above the GS, separated by barriers of 0.554, 0.591 eV (jumps from state 3 to 4 in Fig. 5b are also observed). At 600 K, the characteristic trapping time is about 0.03 μs. The GS being only ∼0.04 eV below the separated C, this state is favored at 600 K for entropic reasons and, the ground state is visited only 11 times (over 3814 KMC steps) during the 80 μs run, while the first excited state, $E_{min} \approx 0.02$ eV above the GS, is sampled 18 times. This explains why, as demonstrated by the folded distance d_{C-C} at 600 K, as shown in Fig. 8, the C atoms generally move independently from each other.

The third regime, finally, is observed when the two carbons are between 7 and 10 Å from each other. At this distance, elastic deformations do not affect significantly the local energy minima, but they affect the energy barrier by as much as ±0.05 eV as seen in

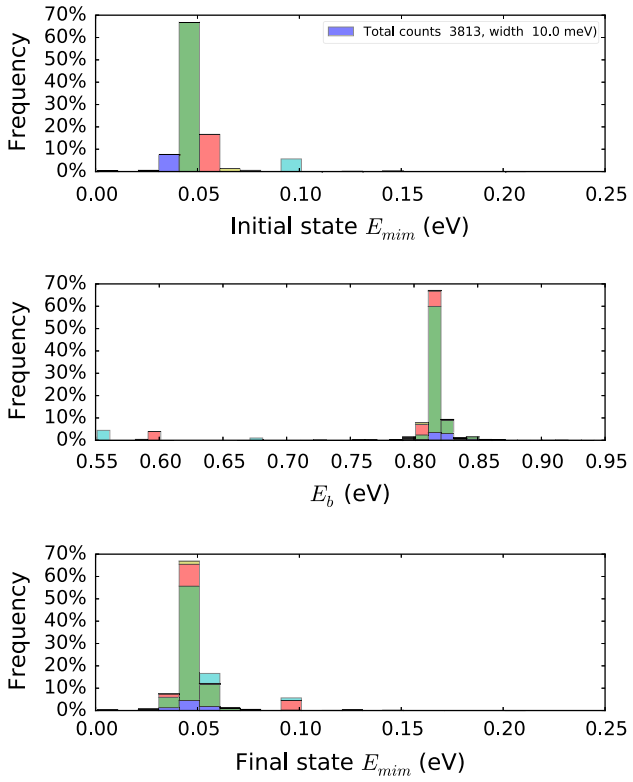

Fig. 9. Histogram of initial, barrier and final energies for 2C interstitials. Each event – characterized by initial, saddle and final energies – is represented with the same color and accumulated in bins. (For interpretation of the references to color in this figure legend, the reader is referred to the web version of this article.)

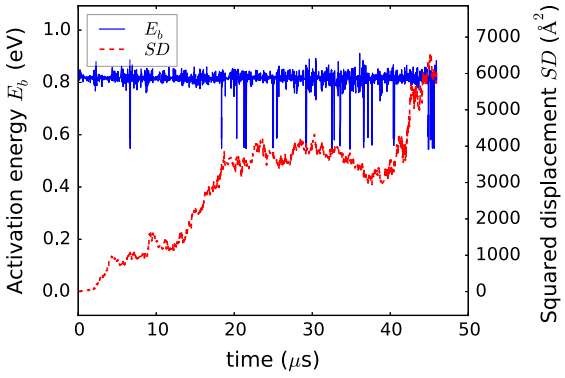

Fig. 10. Migration energies (left axis) and diffusion (right axis) for 4C in interstitial position as a function of time at 600 K for a 2799 KMC step run.

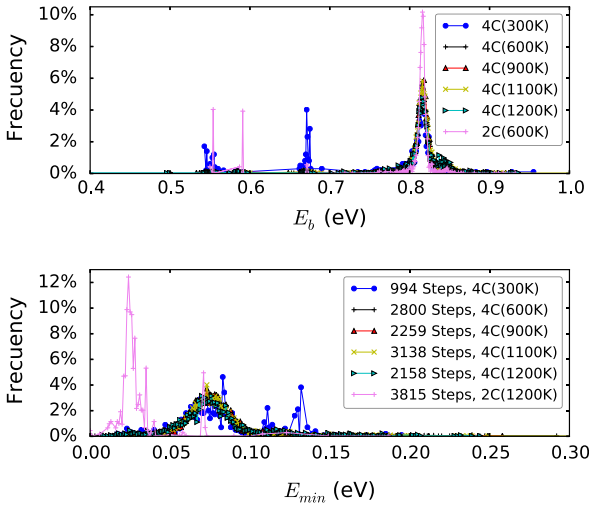

Fig. 12. Top: Barrier energy distributions for five temperatures for the 4C system, with a comparison to the 2C at 600 K. Bottom: Same for the final energy distribution. The respective lowest energy found is subtracted to each data, for 2C is −4129.455 eV while for 4C is −4149.596 eV, and they are separated by 20.161 eV. The bin separation or resolution in E_b and E_{min} is equal to 1 meV.

Fig. 9, with the specific barrier depending on the details of the relative position and the direction of diffusion.

Overall, therefore the C–C complex is too weakly bound to move as a whole and the kinetics, although affected by the presence of nearby C atoms, is fully controlled by single C diffusion.

4.2. Four C interstitials

Here we consider four C atoms randomly placed in interstitial positions in the Fe crystal and let to diffuse at various temperatures. Fig. 10 shows the diffusion and energy barriers at 600 K.

In that figure each consecutive pair of C atoms have the same GS shown in Fig. 5a for the 2C complex. According to Eq. (3), the GS has a binding energy of 0.105 eV, compared with the two isolated C atoms in their GS, and 0.195 eV, compared to four isolated C. The 4C system is characterized by a large number of states with almost degenerate energy where the GS is a symmetric configuration of 4C as shown in Fig. 11.

In view of the small binding energy for four C, diffusion is dominated by the single C barrier (0.817 ± 0.023 eV), but with a broader energy distribution than for the 2C system due to the more complex elastic interactions associated with a higher number of impurities. This is evident in Fig. 12, that presents the distributions of the E_b (top) and E_{min} (bottom) for various temperatures for the 4C system and compares with the similar distributions for the 2C

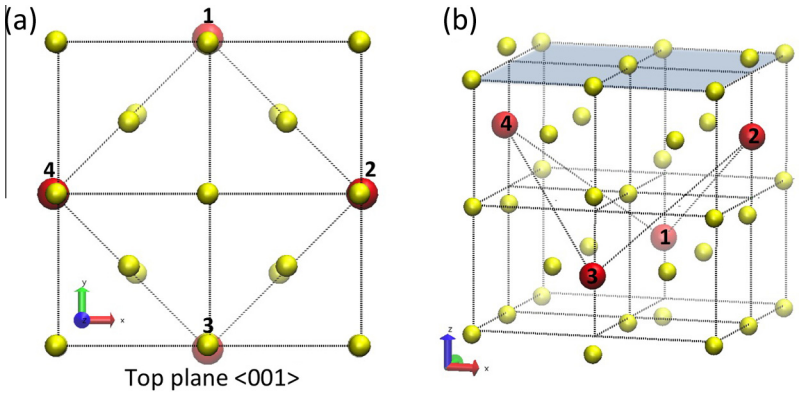

Fig. 11. Ground state of the 4C atom system. (a) top view and (b) 3D view. The distance between the two C, indicated by a line, is $\sqrt{3}a_0$ Å, as in Fig. 5a.

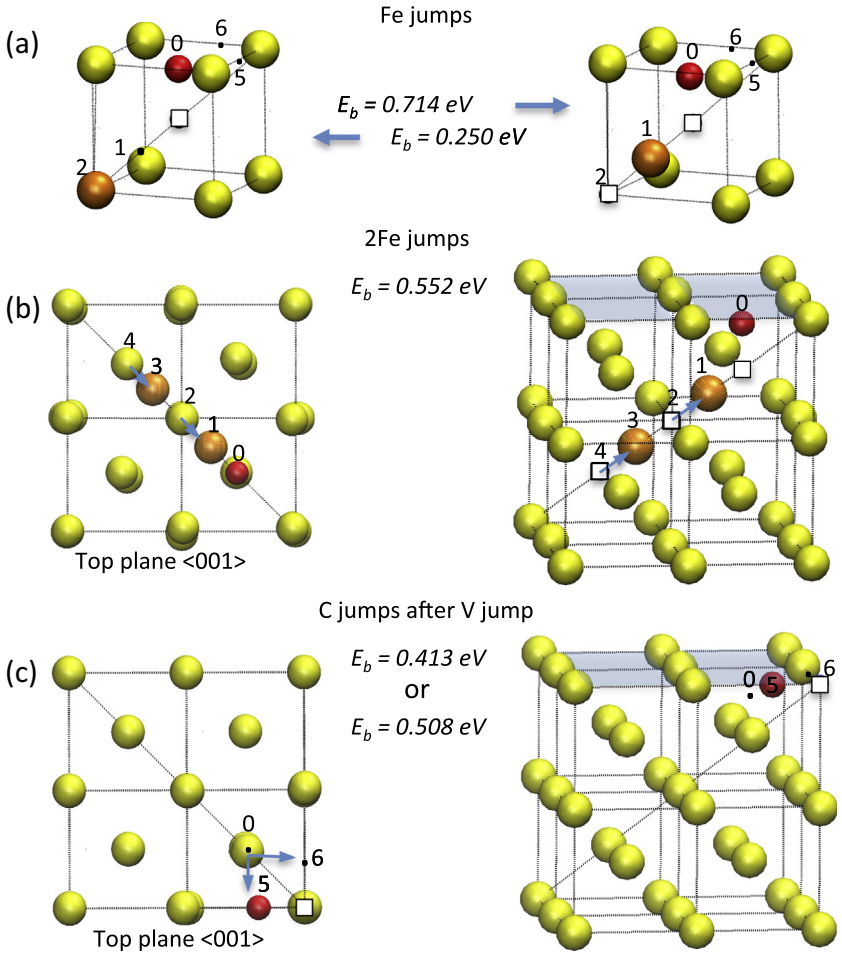

Fig. 13. (a) Jumps of one of the Fe atoms around V at 600 K. (b) Top plane ⟨0 0 1⟩and perspective views of double Fe jumps in a cube with four cells. Orange Fe atoms jump from 4 to 3 and from 2 to 1 (squares are empty crystal sites). In (c) after V moves to the corner, C jumps from position 0 to the edge on position 5, and into the plane around V; position 6 is also possible. The C distance from V is $0.365a_0$; this position is the global minimum: $E_{min} = 0$.

system at 600 K. Because of the large entropy associated with the presence of numerous states of similar energy, the GS is not found in the simulations at 300 K and above; it is generated, however, at a temperature of 50 K.

Fig. 12 also allows us to see that while trapping, associated with two C coming nearby, is significant at lower temperature, with clear peaks for the intra-trap barriers, at 300 K, this attraction becomes negligible at 900 K and above as entropic gain overcomes the small binding energy.

The introduction of more C atoms induces elastic stresses into the Fe crystal, generating a more complex energy landscape without, however, any new dominant mechanism. The wide energy-barrier distribution associated with elastic effects due to the presence of nearby C atoms could be one to the reasons why several values for E_b are observed experimentally between 0.8 and 0.9 eV approximately [22–27].

In this system as in the case of 2C complex, coordinated displacements with four or two C atoms are not observed.

5. Diffusion for systems with vacancy–carbon interactions

5.1. One C in substitutional position

We now look at the effect of substituting one Fe atom in the lattice by a C atom, forming a carbon vacancy complex (V–C) that has been extensively studied using empirical and DFT approaches [12,17,29].

As demonstrated in the literature, a C at a Fe-vacancy lattice point is metastable and, as a consequence, the C atom moves away from it, in an interstitial position, at 1.042 Å from vacancy site, forming a bound state with the self-defect. Indeed, starting with the C in substitutional position, the first KMC event systematically moves this atom over a small barrier, $E_b \approx 0.013$ eV, $(0.365 \pm 0.001)a_0$ away from the vacancy site along of one of the x-axis, into the GS, 1.449 eV below the initial energy, in excellent agreement with results found using DFT [29]. The effect of the vacancy is therefore to bring the C away from the octahedral interstitial site, inside of a cube with the vacancy at the center, (see Fig. 13a).

Doing so, the C stabilizes into a complex that hinders the V diffusion [12]. This stability is particularly evident a room temperatures, as corroborated by the k-ART simulation done at 300 K. This simulation reaches a simulated time of 120 000 s ($\approx$ 33.3 h) in 15 000 steps and shows a V–C system oscillating between nearby positions, but without diffusion (not shown). As the temperature rises, the V–C pair can move either together, as a complex, or can be decoupled, leading to an independent diffusion pathway for both defects. Those effects are observed for simulations at 600 K and above, and are described as follows.

Fig. 13 shows the possible bounded moves for Fe and C around the complex with V-neighboring Fe atoms marked from 1 to 4. With a vacancy nearby, the Fe atoms mostly sample interstitial positions. Single Fe jumps, from GS to an interstitial position 0.463 eV higher, are characterized by a 0.714 eV forward and a 0.251 eV reverse barrier. Two Fe atoms can also make a collective

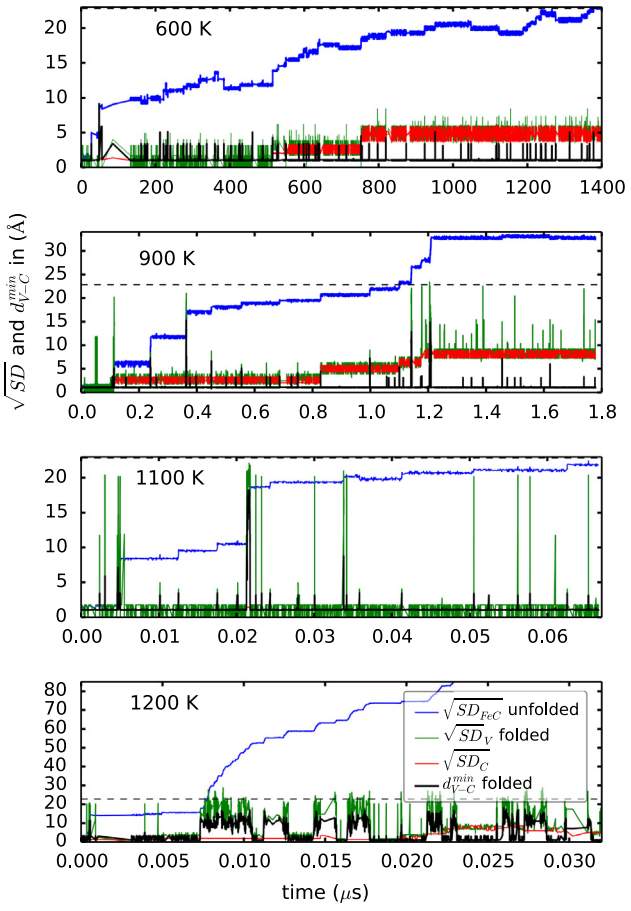

Fig. 14. Roots of the square displacements for vacancies SD_V (folded), for Fe atoms SD_{Fe} and for a C atom SD_C (unfolded), as a function of time. d^{min}_{V-C} is the minimum V–C distance at each step, the lowest value is $0.364a_0$. The horizontal dotted line is the size of box $8a_0 = 22.8$ Å given as a reference.

move to interstitial positions by crossing a 0.552 eV barrier (see Fig. 13b). This motion involves Fe atoms positioned on the same diagonal (direction $\langle 1\,1\,1\rangle$); it is represented by orange atoms, with the empty lattice sites represented as open squares, in Fig. 13. While this event leads to a net mass diffusion, as shown, for example, by the square Fe displacement in Fig. 14a, it leaves the V–C complex unmoved.

Oscillations (or periodic jumps inside the cell) are also observed for the bound C atom with barriers of either $E_b = 0.413$ eV or $E_b = 0.508$ eV (Fig. 13c), in agreement with DFT values of 0.4 eV and 0.6 eV [29]. $E_b = 0.413$ eV corresponds to a situation in which there is an Fe atom at interstitial position (as e.g. Fe at position 1, close to V), allowing C to jump to another octahedral position before the Fe goes back to its initial position (position 0 in Fig. 13a and c). The $E_b = 0.508$ eV is associated to the same C jump, but with all Fe atoms in their initial position.

These moves correspond to the most frequent oscillations observed in Fig 14 for C. This figure presents the evolution of the V–C system at four different temperatures, from 600 to 1200 K. It shows, as a function of time (note the change in time scale as a function of temperature), the minimum V–C distance, d^{min}_{V-C}, as well as the root of the square displacement for Fe atoms (SD_{Fe}), C (SD_C, unfolded) and the vacancy (SD_V, folded). The root of the square displacement is taken to facilitate comparison with d^{min}_{V-C} and the folded SD_V. Using the definition of Section 3.1, a V is created when no atom can be found at a distance of 0.5 Å or less from the lattice site. At each time step, therefore, one, two or three V may be present and the $SD_V(t_n)$ is computed as an average over the number of vacancies found that time step and can be compared with d^{min}_{V-C} to verify the binding of the V–C complex as a function of the temperature.

We first observe that the V–C complex unbinding is a relatively rare event. At 600 K, C diffusion can be observed around 515 μs and 800 μs (green line in Fig. 14 a), and after 0.8 μs at 900 K (Fig. 14b). At 600 and 900 K, the V–C complex moves mostly as a whole, as is shown by d^{min}_{V-C} in the top two panels of Fig. 14. V–C diffusion is also seen in Fig. 15, where these specific regions are highlighted in the

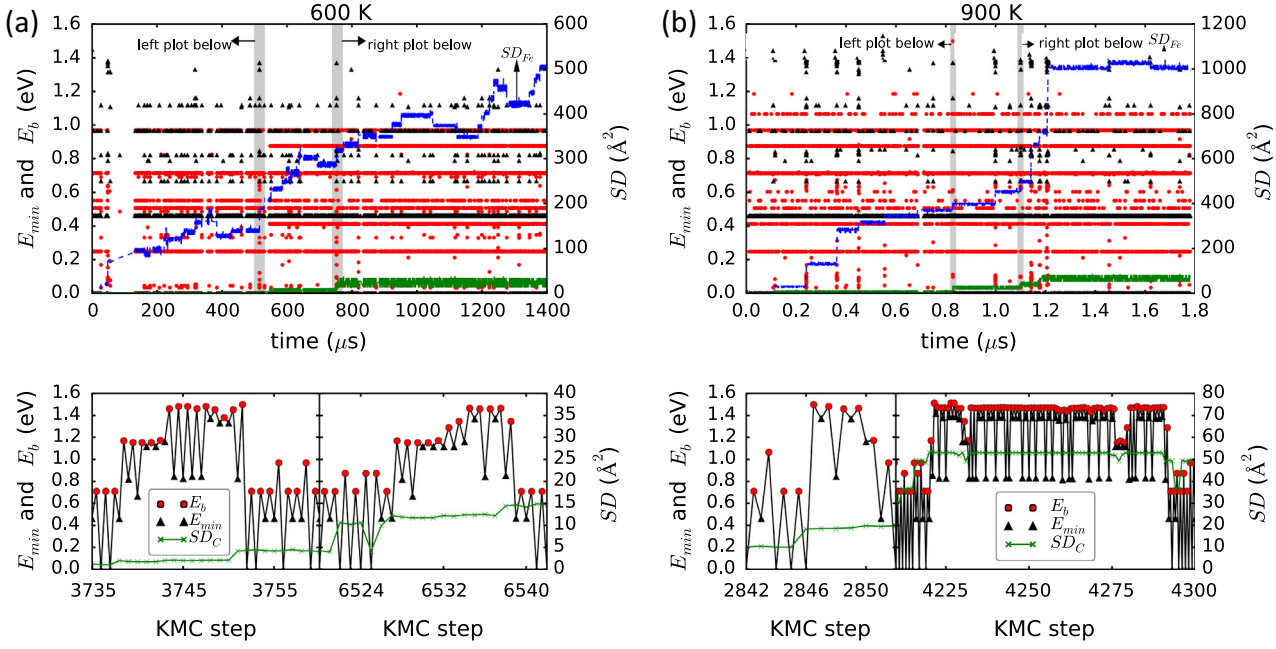

Fig. 15. Top: C (green lines) and Fe (blue line) self-diffusion (right axis) compared to the change in energy, E_{min} (red circles, left axis) and to barrier energies, E_b (black triangles, left axis) at 600 K (a) and 900 K (b). Bottom: zoom on two intervals (gray areas in top) in which C or V diffuse independently. Energies in the bottom panels (a and b) are measured with respect to the ground state. (For interpretation of the references to color in this figure legend, the reader is referred to the web version of this article.)

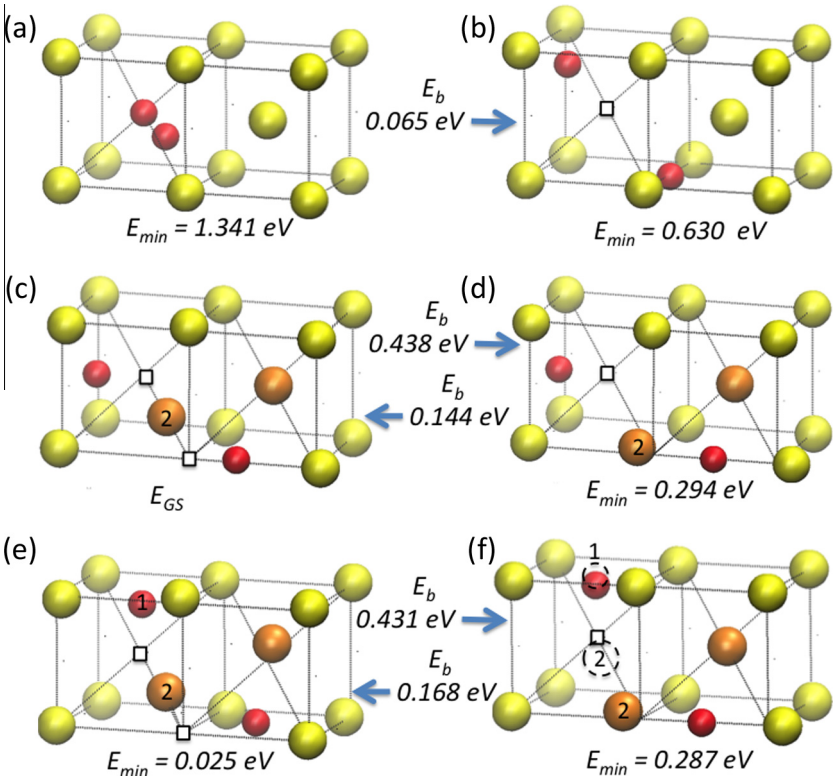

Fig. 16. (a) Initial configuration with 2C inside a vacancy site, after the first energy minimization the system moves to the configuration (b). From (c) the GS, the system may oscillate with state (d). In (e) a second possible configuration, the system can oscillate with state (f). In (f) dashed circles represent another degenerated local configuration in which atoms 1 and 2 of the system can move from (e).

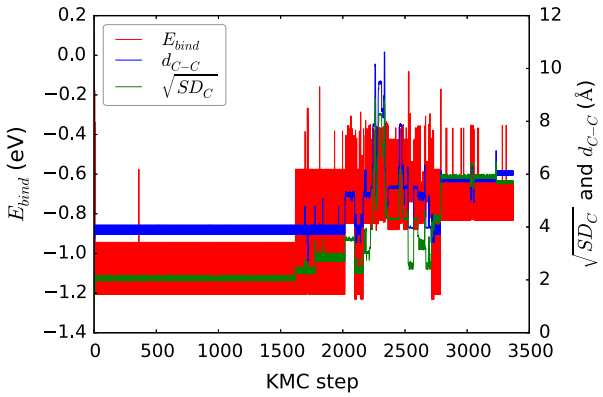

Fig. 17. In left the binding energy, E_{bind}, as a function of KMC steps at 600 K. In right the C–C distance, d_{C-C} and the root of the SD_C.

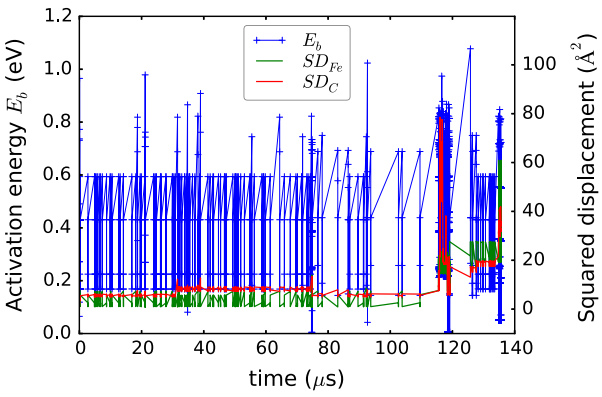

Fig. 18. Migration energy (blue line, left axis) and SD_{Fe} (green line, right axis) and SD_C (red line, right axis), for a V–2C system as a function of time at 600 K for a 3373 KMC step run. (For interpretation of the references to color in this figure legend, the reader is referred to the web version of this article.)

top panels and show in more details, as a function of KMC step, in the bottom panel, where we clearly see the dissociation of the V–C complex. At 600 K, this happens for a few steps (as seen around step 3745 in Fig. 15a).

At 900 K and above, the dissociation is more evident. It can be easily observed at 1200 K, for example, from d^{min}_{V-C} in Fig. 14, that V and C are decoupled most of the time. At this high temperature, the V–C dissociation is crucial for diffusion: as the system decouples, the vacancy moves rapidly across the crystal before it is trapped again by C. V–C complex movement is not a schematic process, i.e., a defined path between two GS configurations cannot be predicted, as it can be deduced when comparing bottom plots of Fig. 15a and b. The V–C complex kinetics can be understood by looking at specific jumps such as the one presented in the right hand side bottom plot of Fig. 15b. After oscillating for 1.1 μs around the V–C complex GS, the system crosses a ∼1.5 eV barrier at KMC step 4219, leading to the dissociation of V–C. This brings the system into an energy state about 0.8 eV above GS, freeing the V that can move across the crystal, with events characteristic of the simple V diffusion, crossing the box boundary to finally be trapped again by the C image at step 4293 when the system returns to the global minimum again. As a whole, therefore, the V–C complex diffusion from one bound GS to another is characterized by an overall energy barrier of 1.5 eV. This energy is confirmed through the use of the statistically exact bac-MRM approach [5], which allows us to repeat this diffusion process while solving statistically for the intermediates steps. With such a high dissociation

Table 1
General properties of C and V for the systems studied using kART. $E_{ref} = -4109.294$ eV is the energy of the perfect crystal. For 2C and 4C, the error is the standard deviation in the convergence or, in the case of V–C, the width of the distribution for various similar pathways (see bottom Fig. 15a and b).

System	E_b	$(E_{GS} - E_{ref})$
C	0.815[a]	−10.058
2C	0.816 ± 0.009	−20.161
4C	0.817 ± 0.023	−40.427
V	0.640[b]	5.734
V–C	1.5 ± 0.02[c]	−5.155
V–2C	1.114[d]	−15.614

[a] Same value of Refs. [33,12].
[b] Same value of Refs. [11,45].
[c] Total barrier for complex diffusion or splitting.
[d] Barrier to decouple one C from complex.

barrier, V–C complex diffusion is a rare event with a characteristic time scale of hours at 300 K, microseconds 900 K and nanoseconds at 1200 K (for instance, in Fig. 14 can be identified two periods of 200 μs and 600 μs at 600 K that reduce to 0.2–0.8 μs at 900 K).

5.2. Two C around of a vacancy (V–2C)

According to DFT, when a second C is added to the previous system, the two C atoms move and bind inside a cell in the vicinity of the V, as shown in Fig. 16a, in agreement with the computed prediction of Domain et al. [29], which states that a vacancy can bind to up to a maximum of two C atoms. This result is corroborated by further computations [17] that show that V–C systems are energetically favorable for systems up to two C, with the two C atoms moving inside the vacancy and forming a covalent C–C bond.

Diffusion mechanisms for two nearby not bonded carbon atoms have not been characterized however, even though these are of fundamental interest in low-concentration C environments. Here, we focus on this situation in which a V interacts with 2C atoms beyond first-neighbor distances.

Simulations on this system show that in the first KMC step (just after energy minimization), starting from the two C into the vacancy site, the C atoms separate with one moving to the edge of cell (see Fig. 16b). Latter and depending of the temperature, after some KMC steps, the V–2C system moves to one of two possible configurations (shown in Fig. 16c and e). One of them is the unbounded GS, which is found in all the simulations and shown in Fig. 16c, with an energy $E_{GS} = -4124.908$ eV. Interesting, the Fe atom (the orange marked with 2, close to the V) oscillates between the GS and the position shown in Fig. 16d representing a mechanism by which the system stabilizes. We also observe a V split at the GS (as well as in other configurations as, e.g., in Fig. 16e). Although this splitting has some resemblance with the splitting mechanism observed in Fig. 2 for the case of one V diffusion, in those cases the Fe atom does not move into the lattice position during the oscillations, as can be seen in Fig. 16d and e. The configuration shown in Fig. 16e happens frequently with oscillations to two possible degenerated transition states, as shown in Fig. 16f.

At 600 K, no Fe or C diffusion is observed, although the system decouples over short periods of time, as seen in Fig. 17 in the 1600–2007 KMC-step interval. That figure also gives the C–C binding energy calculated according to Eq. (3). In fact displacement of the V–2C complex is not observed at any of temperatures used. For the V to move, one of the two carbons must move away, with a barrier energy of ∼1.114 eV, (measured from the GS). Once this happens the system stabilizes to a new set of local minima around ∼0.4 eV above the GS with the decoupled C moving into the crystal. Since the C diffusion barrier, at ∼0.81 eV, is much smaller than the 1.5 eV necessary to break the V–C complex, our simulations are dominated by the first mechanism. The coupled system (at least as shown in Fig. 16e and f) is observed for a period of ∼120 μs. After the system goes to visit new states by crossing divers barriers with small time steps that bans the observation of diffusion process, as seen in Fig. 18 around ∼120 μs or KMC step ∼1600 in Fig. 17.

Simulations at 900 K to 1200 K show the same mechanisms with, of course, more frequency dissociation: decoupling time for one C is reduced to ∼20 ns at 900 K and ∼0.35 ns at 1200 K), allowing for the observation of single C diffusion over the simulated time.

6. Summary and conclusions

Using k-ART we characterize the diffusion mechanisms associated with C in the Fe–C system. Comparing with previously published results, we show that k-ART correctly recovers MD observations such as the energy barriers of 0.815 eV for one C and 0.640 eV for V diffusion in Fe. More complex systems are also analyzed and a number of new results are found for C diluted systems and summarized in Table 1.

For 2C interstitials, a global minimum energy with a C–C distance separation of $\sim\sqrt{3}a_0$ is found, in agreement with previous MD and DFT studies. C–C interactions also produce a rough landscape at small distances, with two metastable bound states separated from the GS with barriers of 0.55 eV and 0.59 eV. At longer distances, although C atoms diffuse by crossing barriers with energies similar to that for one C, elastic deformations due to the presence of a second C induce a distribution around the $E_b = 0.816$ eV. This distribution increases as C atoms are added, which helps to explain the variety of barrier energies observed experimentally. These distributions are more affected by increasing the number of C atoms than by changing the temperature.

The introduction of a vacancy in the presence of a C atom creates a stable V–C complex, that moves as a whole at low-medium temperatures. At 300 K, for example, the V–C complex is stable for periods of time of the order of hours, at 600 K diffusion of the coupled V–C complex, with a 1.5 eV barrier, is observed around 515 μs and 800 μs, while it dissociates above 900 K. In this latter case, V and C diffuse with a barrier energy close to that of the isolated defects until they pass close to each other and get trapped, with a lifetime of ps at 1200 K. In general, dissociation and diffusion of separated V and C take place through several steps, by climbing a number of small barriers in the surface energy that sum up to 1.5 eV, explaining the slow overall diffusion.

As in the case of V–C system, a V–2C complex in conditions where 2C are beyond first-neighbor distance is also created. It is associated with a large number of almost degenerate bound excited states that occupy two cells. This complex is less stable than the V–C complex and a single C unbinds with a 1.11 eV barrier, while in contrast to the V–C, displacement of the V–2C complex is not observed. This mechanism dominates the dynamics in our simulations.

Overall, this work shows both the strength of the kinetic Activation–Relaxation Technique for mapping out complex energy landscapes and identifying the relevant kinetic and the richness of the C-diffusion mechanisms in Fe. With the applicability of the method demonstrated, further work is currently underway for the effects of grain boundaries on defect diffusion.

Acknowledgments

This work is supported by the Qatar National Research Fund (QNRF) through the National Priorities Research Program (NPRP

6-863-2-355). This work has been supported by the Canada Research Chairs program and by grants from the Natural Sciences and Engineering Research Council of Canada (NSERC). We are grateful to *Calcul Québec*/Compute Canada (CQ/CC) for generous allocations of computer resources. The k-ART package is available for distribution by contacting the authors.

References

[1] G.Y. Lai, High-temperature corrosion and materials applications, ASM International, 2007.
[2] A.F. Voter, Phys. Rev. B 34 (1986) 6819, http://dx.doi.org/10.1103/PhysRevB.34.6819.
[3] A. Voter, Radiat. Eff. Solids 235 (2007) 1–23, http://dx.doi.org/10.1007/978-1-4020-5295-8_1.
[4] F. El-Mellouhi, N. Mousseau, L.J. Lewis, Phys. Rev. B 78 (2008) 153202, http://dx.doi.org/10.1103/PhysRevB.78.153202.
[5] L.K. Béland, P. Brommer, F. El-Mellouhi, J.-F. Joly, N. Mousseau, Phys. Rev. E 84 (2011) 046704, http://dx.doi.org/10.1103/PhysRevE.84.046704.
[6] N. Mousseau, L.K. Béland, P. Brommer, F. El-Mellouhi, J.-F. Joly, G.K. N'Tsouaglo, O. Restrepo, M. Trochet, Comput. Mater. Sci. 100, Part B (0) (2015) 111–123, http://dx.doi.org/10.1016/j.commatsci.2014.11.047. Special Issue on Advanced Simulation Methods. <http://www.sciencedirect.com/science/article/pii/S0927025614008271>.
[7] L.K. Béland, Y.N. Osetsky, R.E. Stoller, H. Xu, Phys. Rev. B 91 (2015) 054108, http://dx.doi.org/10.1103/PhysRevB.91.054108. <http://link.aps.org/doi/10.1103/PhysRevB.91.054108>.
[8] L.K. Béland, Y. Anahory, D. Smeets, M. Guihard, P. Brommer, J.-F. m. c. Joly, J.-C. Pothier, L.J. Lewis, N. Mousseau, F.m.c. Schiettekatte, Phys. Rev. Lett. 111 (2013) 105502, http://dx.doi.org/10.1103/PhysRevLett.111.105502. <http://link.aps.org/doi/10.1103/PhysRevLett.111.105502>.
[9] J.-F. Joly, L.K. Béland, P. Brommer, N. Mousseau, Phys. Rev. B 87 (2013) 144204, http://dx.doi.org/10.1103/PhysRevB.87.144204. <http://link.aps.org/doi/10.1103/PhysRevB.87.144204>.
[10] P. Brommer, N. Mousseau, Phys. Rev. Lett. 108 (2012) 219601, http://dx.doi.org/10.1103/PhysRevLett.108.219601.
[11] P. Brommer, L.K. Béland, J.-F. m. c. Joly, N. Mousseau, Phys. Rev. B 90 (2014) 134109, http://dx.doi.org/10.1103/PhysRevB.90.134109.
[12] K. Tapasa, A.V. Barashev, D.J. Bacon, Y.N. Osetsky, Acta Mater. 55 (1) (2007) 1–11, http://dx.doi.org/10.1016/j.actamat.2006.05.029.
[13] D. Terentyev, N. Anento, A. Serra, V. Jansson, H. Khater, G. Bonny, J. Nucl. Mater. 408 (3) (2011) 272–284, http://dx.doi.org/10.1016/j.jnucmat.2010.11.053.
[14] A. Ishii, S. Ogata, H. Kimizuka, J. Li, Phys. Rev. B 85 (6) (2012) 1–7, http://dx.doi.org/10.1103/PhysRevB.85.064303.
[15] V. Jansson, L. Malerba, J. Nucl. Mater. 443 (1–3) (2013) 274–285, http://dx.doi.org/10.1016/j.jnucmat.2013.07.046.
[16] D. Terentyev, I. Martin-Bragado, Scr. Mater. 97 (2015) 5–8. <http://www.sciencedirect.com/science/article/pii/S1359646214004291>.
[17] C.C. Fu, E. Meslin, A. Barbu, F. Willaime, V. Oison, Solid State Phenom. 139 (2008) 157–164, http://dx.doi.org/10.4028/www.scientific.net/SSP.139.157.
[18] L. Zhang, C.C. Fu, G.H. Lu, Phys. Rev. B 87 (13) (2013) 1–11, http://dx.doi.org/10.1103/PhysRevB.87.134107.
[19] H. Bhadeshia, J. Mater. Sci. 39 (12) (2004) 3949–3955, http://dx.doi.org/10.1023/B:JMSC.0000031476.21217.fa.
[20] H. Bhadeshia, Philos. Mag. 93 (28–30) (2013) 3714–3725, http://dx.doi.org/10.1080/14786435.2013.775518. <http://www.tandfonline.com/doi/abs/10.1080/14786435.2013.775518>.
[21] D. Terentyev, K. Heinola, A. Bakaev, E. Zhurkin, Scr. Mater. 86 (2014) 9–12, http://dx.doi.org/10.1016/j.scriptamat.2014.04.003. <http://www.sciencedirect.com/science/article/pii/S1359646214001481>.
[22] C.A. Wert, Phys. Rev. 79 (1950) 601–605, http://dx.doi.org/10.1103/PhysRev.79.601. <http://link.aps.org/doi/10.1103/PhysRev.79.601>.
[23] G.G. Tibbetts, J. Appl. Phys. 51 (9) (1980) 4813–4816, http://dx.doi.org/10.1063/1.328314.
[24] Y. Iijima, J. Alloys Compd. 234 (2) (1996) 290–294, http://dx.doi.org/10.1016/0925-8388(95)02104-3. <http://www.sciencedirect.com/science/article/pii/0925838895021043>.
[25] R. McLellan, M. Wasz, J. Phys. Chem. Solids 54 (5) (1993) 583–586, http://dx.doi.org/10.1016/0022-3697(93)90236-K. <http://www.sciencedirect.com/science/article/pii/002236979390236K>.
[26] A.D. LeClaire, in: H. Mehrer (Ed.), Landolt-Börnstein, Numerical Data and Functional Relationships in Science and Technology, New Series, Group III: Crystal and Solid State Physics, 26, 1990, pp. 480–481, http://dx.doi.org/10.1007/10390457_90. <http://materials.springer.com/lb/docs/sm_lbs_978-3-540-46109-8_90>.
[27] S. Takaki, J. Fuss, H. Kuglers, U. Dedek, H. Schultz, Radiat. Eff. 79 (1–4) (1983) 87–122, http://dx.doi.org/10.1080/00337578308207398.
[28] W. Choo, R. Kaplow, Acta Metall. 21 (6) (1973) 725–732, http://dx.doi.org/10.1016/0001-6160(73)90036-9. <http://www.sciencedirect.com/science/article/pii/0001616073900369>.
[29] C. Domain, C.S. Becquart, J. Foct, Phys. Rev. B 69 (2004) 144112, http://dx.doi.org/10.1103/PhysRevB.69.144112. <http://link.aps.org/doi/10.1103/PhysRevB.69.144112>.
[30] R. Johnson, G. Dienes, A. Damask, Acta Metall. 12 (11) (1964) 1215–1224, http://dx.doi.org/10.1016/0001-6160(64)90105-1. <http://www.sciencedirect.com/science/article/pii/0001616064901051>.
[31] D.S. Tchitchekova, J. Morthomas, F. Ribeiro, R. Ducher, M. Perez, J. Chem. Phys 141 (3) (2014), http://dx.doi.org/10.1063/1.4889854.
[32] C. Becquart, J. Raulot, G. Bencteux, C. Domain, M. Perez, S. Garruchet, H. Nguyen, Comput. Mater. Sci. 40 (1) (2007) 119–129, http://dx.doi.org/10.1016/j.commatsci.2006.11.005.
[33] R. Veiga, C. Becquart, M. Perez, Comput. Mater. Sci. 82 (0) (2014) 118–121, http://dx.doi.org/10.1016/j.commatsci.2006.11.005.
[34] B.D. McKay, Congressus Numerantium 30 (1981) 45–87. <http://cs.anu.edu.au/bdm/nauty>.
[35] B.D. McKay, A. Piperno, J. Symb. Comput. 60 (2014) 94–112, http://dx.doi.org/10.1016/j.jsc.2013.09.003. <http://www.sciencedirect.com/science/article/pii/S0747717113001193>.
[36] B. Puchala, M.L. Falk, K. Garikipati, J. Chem. Phys. 132 (2010) 134104, http://dx.doi.org/10.1063/1.3369627.
[37] M. Mendelev, S. Han, D. Srolovitz, G. Ackland, D. Sun, M. Asta, Philos. Mag. 83 (35) (2003) 3977–3994, http://dx.doi.org/10.1080/14786430310001613264.
[38] R. Veiga, M. Perez, C. Becquart, E. Clouet, C. Domain, Acta Mater. 59 (18) (2011) 6963–6974, http://dx.doi.org/10.1016/j.actamat.2011.07.048.
[39] R.G.A. Veiga, M. Perez, C.S. Becquart, C. Domain, J. Phys. Condens. Matter 25 (2) (2013) 025401, http://dx.doi.org/10.1088/0953-8984/25/2/025401. <http://stacks.iop.org/0953-8984/25/i=2/a=025401>.
[40] N. Gunkelmann, H. Ledbetter, H.M. Urbassek, Acta Mater. 60 (12) (2012) 4901–4907, http://dx.doi.org/10.1016/j.actamat.2012.05.038. <http://www.sciencedirect.com/science/article/pii/S1359645412003588>.
[41] S. Plimpton, J. Comput. Phys. 117 (1995) 1, http://dx.doi.org/10.1006/jcph.1995.1039.
[42] Lammps web site. <http://lammps.sandia.gov/index.html>
[43] C. Wert, C. Zener, Phys. Rev. 76 (1949) 1169–1175, http://dx.doi.org/10.1103/PhysRev.76.1169. <http://link.aps.org/doi/10.1103/PhysRev.76.1169>.
[44] G.H. Vineyard, J. Phys. Chem. Solids 3 (1–2) (1957) 121–127, http://dx.doi.org/10.1016/0022-3697(57)90059-8. <http://www.sciencedirect.com/science/article/pii/0022369757900598>.
[45] L. Malerba, M.C. Marinica, N. Anento, C. Björkas, H. Nguyen, C. Domain, F. Djurabekova, P. Olsson, K. Nordlund, A. Serra, D. Terentyev, F. Willaime, C.S. Becquart, J. Nucl. Mater. 406 (1) (2010) 19–38, http://dx.doi.org/10.1016/j.jnucmat.2010.05.017.
[46] D.E. Jiang, E.A. Carter, Phys. Rev. B 67 (2003) 214103, http://dx.doi.org/10.1103/PhysRevB.67.214103. <http://link.aps.org/doi/10.1103/PhysRevB.67.214103>.